sciendo

Geologos 31, 3 (2025): 183–199
https://doi.org/10.14746/logos.2025.31.3.15

GEOLOGOS

Identifying potential groundwater recharge zones using the Analytic Hierarchy Process (AHP) method, in the Upper-Middle Drâa Basin, Morocco

Ghachoui Hayat*, Tabit Adbelhalim, Algouti Ahmed, Errami Maryam, Moujane Said

Department of Geology, Cadi Ayyad University, Faculty of Sciences, University, Morocco
* corresponding author; e-mail: h.ghachoui.ced@uca.ac.ma

Abstract

Groundwater is a vital resource sustaining domestic supply, agriculture, and industry, particularly in arid regions where water scarcity severely limits development. Identifying potential groundwater recharge zones is therefore essential for the sustainable management of this resource. This study assesses the spatial distribution of groundwater recharge potential in the Upper-Middle Drâa Basin, southeastern Morocco, which extends over approximately 23,000 km^2. The Analytic Hierarchy Process (AHP) was applied within a Geographic Information System (GIS) framework using multi-source geospatial data, including Sentinel-2 imagery and the Advanced Spaceborne Thermal Emission and Reflection Radiometer (ASTER) Digital Elevation Model. The results indicate that high-recharge zones are mainly concentrated in low-slope alluvial plains and along major drainage networks, whereas the surrounding highlands exhibit moderate to low recharge potential. Validation using field data from borehole discharge measurements confirms this spatial pattern, with flow rates ranging from about 1.5 L/s in peripheral sectors to over 6 L/s in central parts of the basin. The strong agreement between model outputs and field observations demonstrates the reliability of the adopted approach and enhances understanding of the basin's hydrogeological functioning. Overall, this work provides an effective decision-support tool for regional water resource planning and sustainable groundwater management in arid and semi-arid environments.

Keywords: Hydrogeology, multi-criteria analysis, geospatial modelling

1. Introduction

Water scarcity is becoming one of the most pressing challenges in arid and semi-arid regions, where the pressure on groundwater has intensified due to population growth, expanding agricultural demand, and increasing climatic variability (Priyan, 2021). Identifying regions with potential for groundwater extraction is therefore crucial for sustainable water resource management, particularly in arid regions like the Upper-Middle Drâa Basin. In such environments, the ability to locate areas that naturally favour infiltration is essential for maintaining aquifer stability and ensuring long-term water security. Traditionally, this process has relied on advanced geophysical methods, such as electrical resistivity and seismic refraction, which enable researchers to examine subsurface formations and pinpoint aquifer locations (Bouchaou et al., 2009). However, these techniques are often expensive, limiting their feasibility for broader or long-term applications (Kumar & Ahmed, 2003). To address

these challenges, alternative methods that are both economical and precise have gained increasing attention. In this regard, integrating remote sensing approaches with geographic information systems (GIS) represents a major innovation in groundwater research. Remote sensing offers extensive data coverage across large areas, while GIS facilitates the layering, analysis, and visualisation of spatial data. This combination provides decision-makers with dependable and comprehensive datasets, enabling them to make informed choices about groundwater resource management (Machiwal et al., 2011; Oikonomidis et al., 2015). This interdisciplinary approach fosters closer collaboration between scientists and policymakers, bridging the gap between scientific analysis and practical implementation. In doing so, it supports more sustainable and effective planning for water resources (Lee & Pradhan, 2007). Within this geospatial framework, the Analytic Hierarchy Process (AHP), a multicriteria decision-making method developed by Saaty & Wind (1980), has become widely used in groundwater studies because it assigns consistent weights to geological, geomorphological, hydrological, and climatic factors. Its effectiveness has been demonstrated in several arid and semi-arid environments, including applications in the Western Ghats of India (Arulbalaji et al., 2019), the Main Ethiopian Rift (Diriba et al., 2024), the semi-arid Golina Basin (Gebru et al., 2020), and the San Luis Potosí Basin in Mexico (Uc Castillo et al., 2022). These studies collectively highlight the reliability of the AHP framework for mapping groundwater-favourable zones across large heterogeneous basins. The aim of this study is to pinpoint potential groundwater recharge zones within the Upper-Middle Drâa Basin through the use of the Analytic Hierarchy Process (AHP) and a weighted-overlay analysis tool. This method has already been validated by several previous studies (Sener & Davraz, 2013; Hairchi et al., 2025), which have demonstrated its effectiveness in mapping high-potential areas. Moreover, this method adopts a multidimensional approach, considering geological, topographic, climatic, and soil characteristics (Saaty & Wind, 1980), which significantly enhances the accuracy and reliability of mapping high-potential areas. In contrast to earlier applications, the present study integrates Sentinel-2 multispectral indicators, ASTER-DEM-derived topographic parameters, and local hydrogeological constraints, and focuses specifically on recharge processes rather than groundwater exploitation within a hyper-arid Moroccan basin. This provides a refined spatial understanding of recharge dynamics and delivers a robust scientific basis for sustainable groundwater-management strategies.

2. Study area

The Upper-Middle Drâa Basin (Fig.1) lies in southeastern Morocco, between 31°00' and 32°00' N and

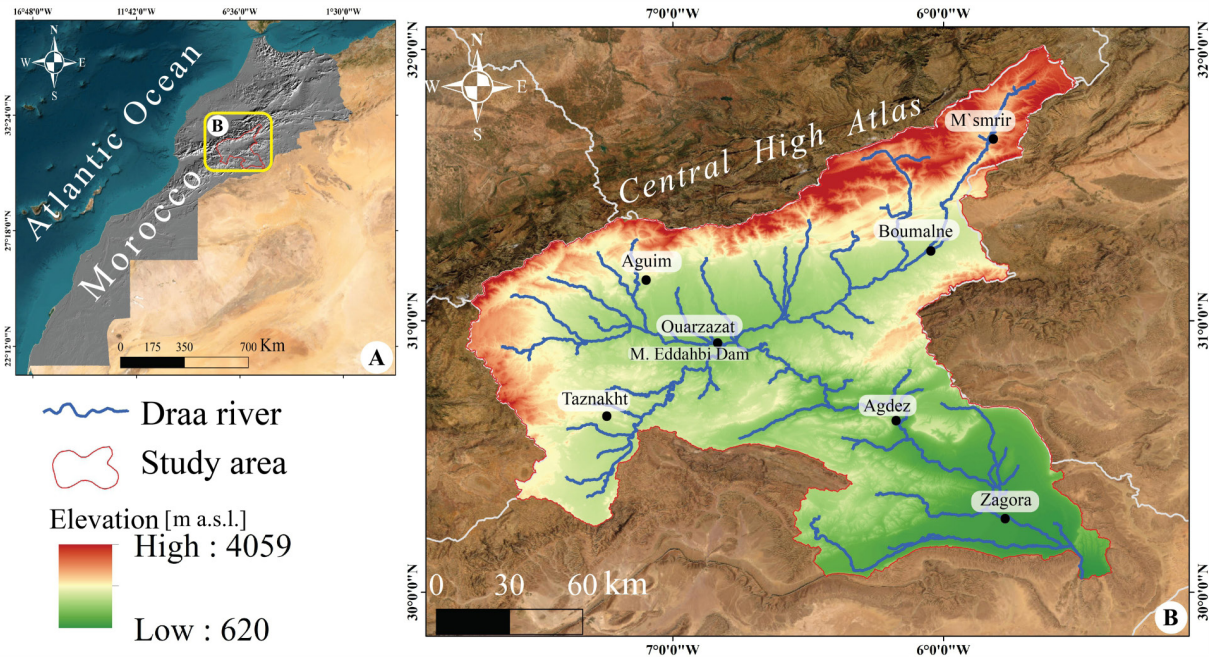

Fig. 1. Location of the study area. **A –** Geographic context within Morocco; **B –** The upper-middle Drâa Basin boundaries.

5°00' and 6°00' W, and covers an area of approximately 23,000 km². It occupies the southern foothills of the Central High Atlas, where elevation rises sharply from the downstream plains (≈620 m) to the highest peaks exceeding 4,000 m. Climatically, the region is governed by an arid to semi-arid regime marked by low annual rainfall, strong seasonal contrasts, and pronounced interannual variability (Agoussine et al., 2004; Benchattou & El Ghachi, 2024). Precipitation is largely concentrated in the northern mountain belt, whereas the central and southern plains remain extremely dry for most of the year. Temperature ranges are considerable, with cold winters in the High Atlas and very hot summers along the Drâa valley. The hydrographic network is structured around the Drâa River, which forms the principal axis of the basin.

2.1. Geological framework

The geology of the Upper-Middle Drâa (Fig. 2) Basin shows a marked north-south transition, beginning in the southern flank of the Central High Atlas, where extensive Meso-Cenozoic formations dominate the landscape. These units, ranging from the Triassic to the Quaternary, include thick sequences of limestones, dolomites, marls, sandstones and siltstones that reflect the long sedimentary and tectonic evolution of the Atlas domain (Schiavo et al., 2007; Benvenuti et al., 2017). Moving southwards, this structured Atlas relief gives way to the broad Neogene-Quaternary depression of Ouarzazate, a tectono-sedimentary basin filled with Mio-Pliocene conglomerates, lacustrine deposits, sandy-silty layers and widespread alluvial formations (Jossen &

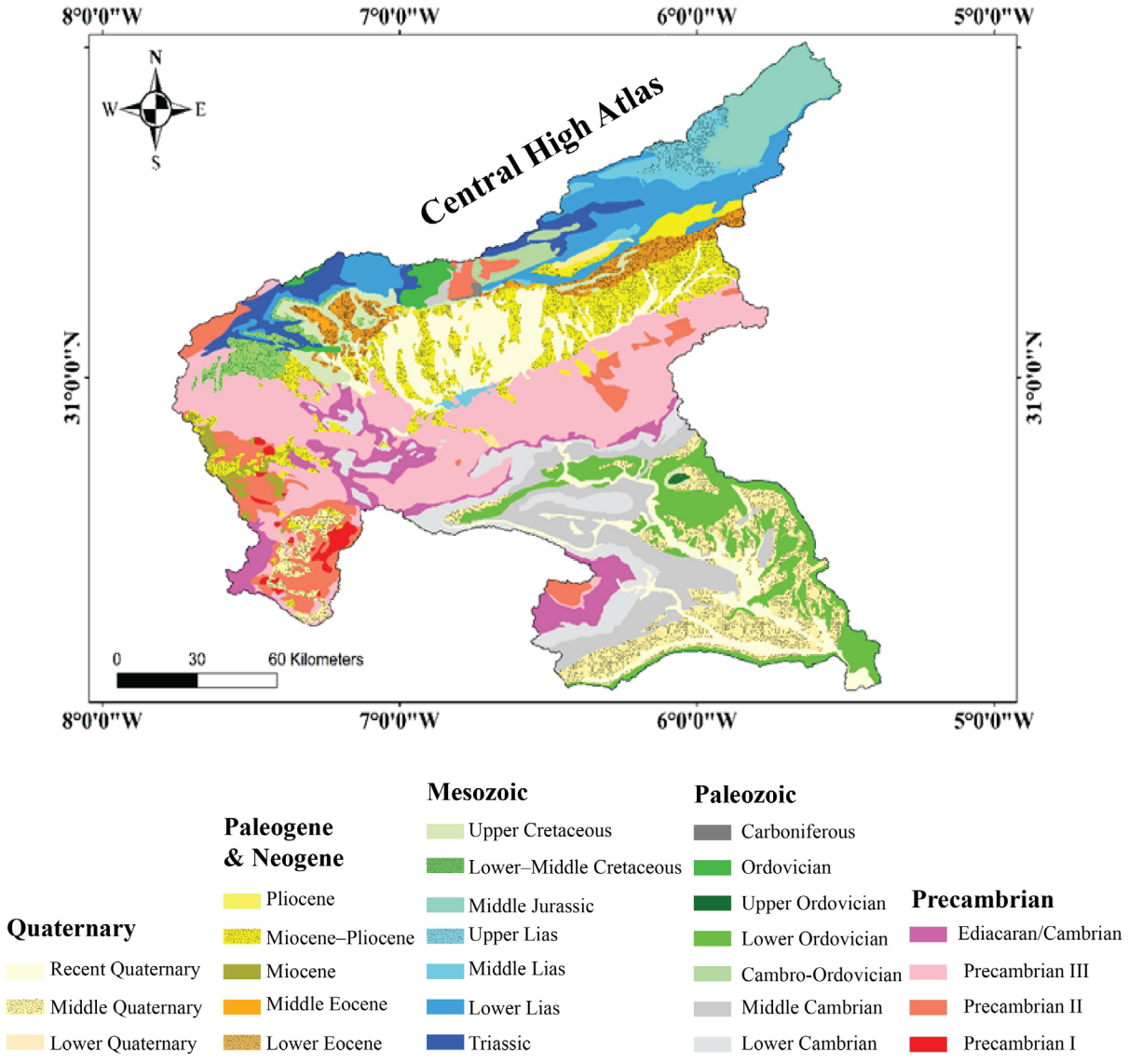

Fig. 2. Geological map of the Upper–Middle Drâa Basin.

Filali Moutei, 1988). These deposits form a transitional zone between the uplifted Atlas chain and the older terrains of the Anti-Atlas. Further south, the geological framework shifts abruptly to the Precambrian basement of the eastern Anti-Atlas, where volcanic, volcaniclastic, magmatic and metamorphic rocks crop out in large inliers. These ancient massifs are encircled by a Palaeozoic sedimentary cover composed of schists, quartzites, sandstones and shale-sandstone alternations extending from the Cambrian to the Carboniferous (Fekkak, 1992; Tuduri et al., 2018; Oukhro et al., 2025). This juxtaposition of Meso-Cenozoic, Neogene-Quaternary and Precambrian-Palaeozoic domains creates a highly heterogeneous geological mosaic characterised by strong lithological contrasts and a wide variety of rock types. Such variability, combined with the pronounced topographic gradients of the region, underpins the geomorphological diversity of the basin and influences processes such as erosion, runoff organisation and material transport (Ervin & Morgan, 2001; Moges & Bhat, 2017).

2.2. Hydrogeological framework

The hydrogeology of the Upper-Middle Drâa is shaped by the strong contrast between the fractured reliefs of the High Atlas to the north and the arid plains of the Anti-Atlas to the south, where groundwater circulates through a mosaic of alluvial, consolidated, and fractured aquifers (Cappy, 2006). The Plio-Quaternary alluvial aquifers form the principal groundwater reservoirs of the basin. Developed along the valley floors of the Drâa River and its tributaries, these aquifers consist of highly permeable gravel, coarse sand, and conglomerate deposits. They maintain direct hydraulic connectivity with surface flows and are replenished during flood events, by deep subsurface inputs from the High Atlas, and through irrigation return flows within oasis systems (DRPE, 1994, 2010). The main aquifer units Dadès-M'Goun, Skoura, Tikert, Ouarzazate, Taznakht, Mezguita, Tinzouline, and Ternata are compartmentalized by a succession of structural thresholds ("foums") described by Jossen & Filali-Moutei (1988), resulting in semi-independent hydrogeological behaviours despite an overall longitudinal continuity along the Drâa valley. The hydrogeological map produced (Fig. 3), based on piezometric data from the Agence du Bassin Hydraulique Drâa-Oued Noun (AHBDON), illustrates the spatial distribution of permeability classes, the layout of isopiestic contours, and the extent of the alluvial aquifers. Depth-to-water values range from 4 to 26 m across the basin, reflecting the pronounced

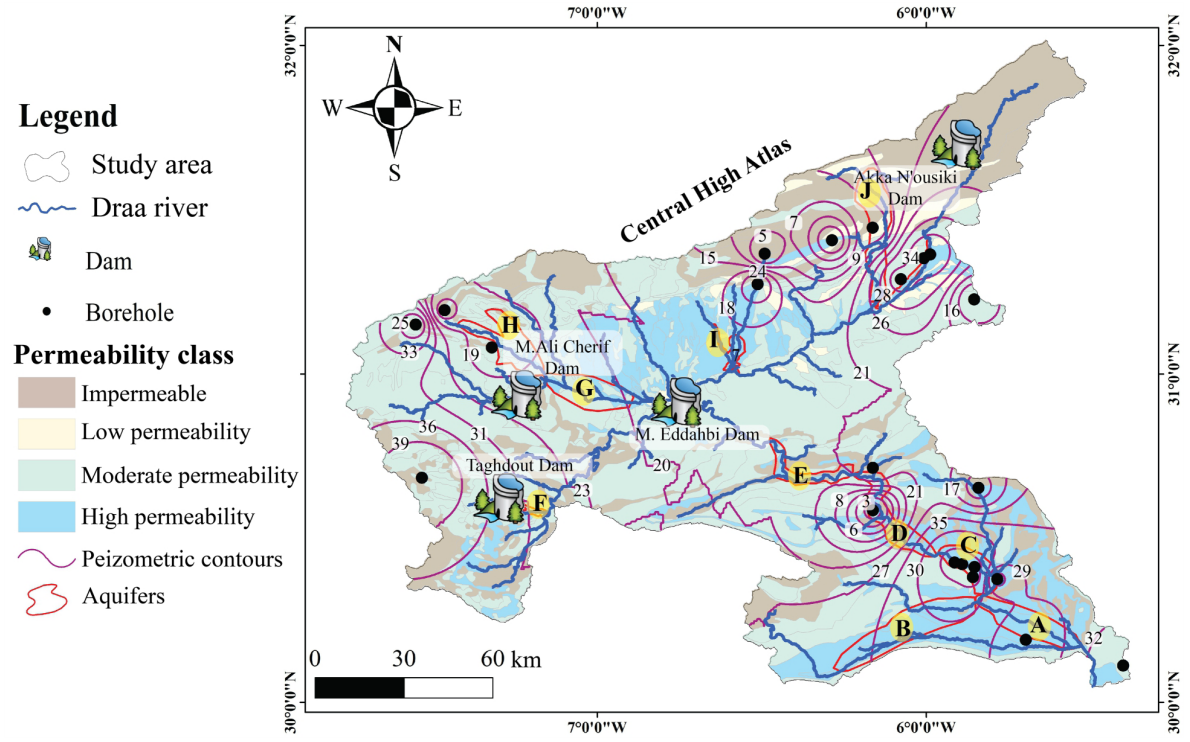

Fig. 3. Hydrogeological map of the Upper–Middle Drâa Basin. Additional explanations: A – Mezguita, B – Foum Zagora Aquifer, C – Ternata Aquifer, D – Tinzouline Aquifer, E – Mezguita Aquifer, F – Taznakht Aquifer, G – Ouarzazate Aquifer, H – Tikirt Aquifer, I – Skoura Aquifer.

heterogeneity of these alluvial systems. Regional data from AHBDON also indicate that borehole yields typically range from 0.8 to 8 L/s, consistent with the hydrodynamic properties of coarse, variably transmissive deposits. Upstream, the limestones and dolomites of the High Atlas form the main recharge areas of the basin. Their dense fracturing promotes deep infiltration, which sustains the Dadès-M'Goun and Skoura aquifers, where groundwater flows through coarse alluvial bodies connected to tributary channels (DRPE, 1994, 2010). Farther west, the Ouarzazate-Tikert and Taznakht aquifers, developed within high-basin alluvial deposits, receive a more irregular recharge that depends largely on mountain runoff and episodic flood events. Downstream, in the Middle Drâa, the Mezguita, Tinzouline, Ternata, and Fezouata aquifers occur within Quaternary alluvium overlying a Palaeozoic schist-quartzite basement; they generally exhibit shallow water levels and show increasing salinity toward the lower valley (DRPE, 1994, 2010).

3. Materials and method

3.1. Datasets

We compiled a comprehensive geospatial dataset describing the environmental factors that control groundwater occurrence in the Upper-Middle Drâa Basin. The dataset includes land-use and land-cover information, topographic parameters, geological and soil units, and long-term climatic records. All spatial layers were standardized to a 30 m resolution and projected in EPSG:4326 to ensure consistency throughout the analytical workflow. Validation data comprising groundwater levels and borehole discharge measurements were obtained from the ABHDON. Land-use/land-cover (LULC) was derived from Sentinel-2 MSI (Level 1C) imagery after applying the QA60 mask to remove clouds and shadows, followed by the creation of a 10 m median composite. Topographic variables were generated from the ASTER GDEM v3 (~30 m). Monthly precipitation series were extracted from the NASA POWER database (https://power.larc.nasa.gov/) and processed to produce continuous climatic surfaces. Geological and soil information was digitized from official map sheets covering the study area, including the Jbel Saghro-Dadès sheet (1:200,000) and the Imiter and Boumalne sheets (1:50,000). All raster layers were resampled, snapped to the DEM grid, and spatially aligned to avoid interpolation artefacts. Groundwater potential zones were delineated using a multi-criteria decision-making (MCDA) framework based on the Analytical Hierarchy Process (AHP). This method was selected for its capacity to structure complex environmental problems, integrate heterogeneous datasets, and provide a transparent weighting of controlling parameters. AHP is widely applied in hydrogeological studies because it supports objective and reproducible ranking of influencing factors (Arulbalaji et al., 2019; Murmu et al., 2019; Gintamo et al., 2022). Its relevance has also been demonstrated in contexts where data availability is limited or where traditional field investigations are costly and time-consuming (Tolche, 2021; Duguma & Duguma, 2022; Olubusola et al., 2023). In this study, combining MCDA-AHP with GIS provided an effective and robust framework for identifying groundwater

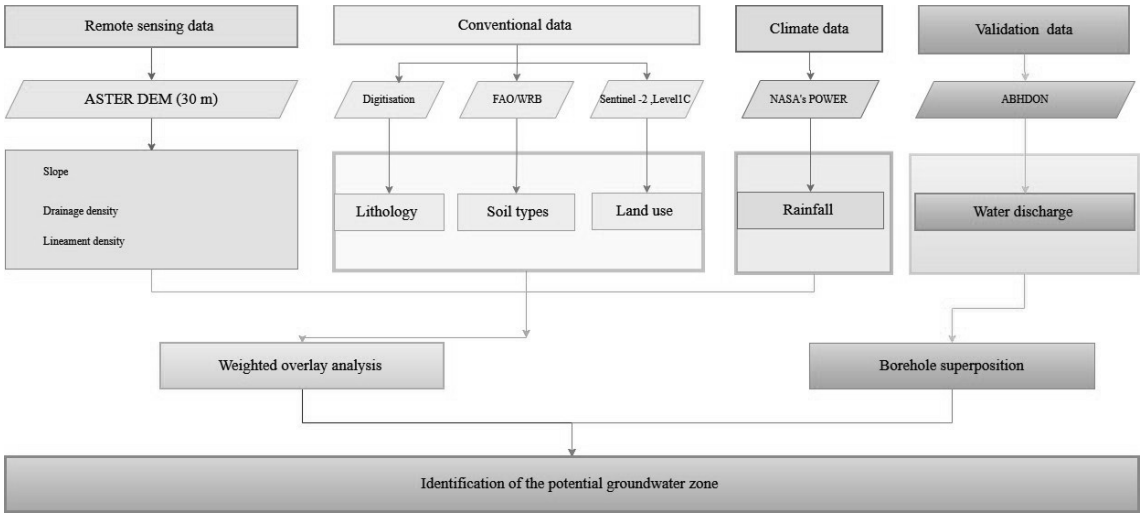

Fig. 4. Flowchart illustrating the methodology adopted in the present study.

potential zones in a geomorphologically diverse and climatically contrasted environment such as the Upper-Middle Drâa basin. The methodological process is illustrated in the flowchart shown in Figure 4.

3.2. Preparation of conditioning factors

3.2.1. Drainage density

We used ASTER GDEM v3 (ASTGTM; 1″ ≈ 30 m) to derive hydrologic surfaces. From the DEM, flow direction and flow accumulation raster were computed; channels were delineated by an accumulation threshold, raster streams were vectorized, and the drainage network was cleaned topologically. Drainage density integrates relief dissection and influences runoff-infiltration partitioning. Drainage density was then calculated as total channel length per unit area:

$$D_d \frac{\sum_j Lj}{A} \tag{1}$$

where:
- D_d – drainage density of the mapping unit (basin, sub-basin, or moving window) [km^{-1}],
- $\sum jLj$ – length of stream segment j that lies inside the mapping unit; measure along the polyline centerline [km],
- A – area of the mapping unit [km^2].

3.2.2. Slope

The slope map was generated from ASTER GDEM v3 (≈30 m resolution), capturing terrain variations that affect runoff and infiltration. Slope gradients were calculated in ArcGIS using the Slope tool (percent units); steep slopes promote runoff, whereas gentle slopes favour infiltration. The resulting raster was reclassified into slope classes to support groundwater-recharge analysis and land-use planning. Slope was computed using a 3 × 3 finite-difference operator. In Horn's formulation:

$$slope_{deg} = arctan\left(\sqrt{(p^2 + q^2)}\frac{180}{\pi}\right) \tag{2}$$

where:
- $p = \partial z / \partial x$ and $q = \partial z / \partial y$ are estimated from the DEM neighbourhood,
- $p = \partial z / \partial x$ (east-west gradient), $q = \partial z / \partial y$ (north-south gradient).

3.2.3. Lineament density

Lineaments, representing linear or curvilinear surface features linked to faults and fractures, indicate structural zones of enhanced permeability and secondary porosity. In hard-rock terrains, they play a key role in groundwater movement and storage. Using ASTER GDEM v3 (≈30 m), lineaments were delineated through DEM-based analysis and GIS processing. Topographic shading and imagery were used to map lineaments (linear or gently curvilinear features indicative of structural weakness). Polylines were converted to density using a moving-window length-per-area definition:

$$L^d = \sum_{i=1}^{n}\left(\frac{L_i}{A}\right) \tag{3}$$

where:
- L^d – lineament density of the mapping unit (sub-basin, polygon, or analysis window) [km^{-1}],
- Li – length of lineament segment i that lies inside the mapping unit [km],
- A – area of the mapping unit [km^2].

As higher densities often indicate enhanced secondary porosity/permeability in hard-rock terrains.

3.2.4. Lithology and soils

The soil settings were derived from FAO/WRB soil classes. To ensure compatibility with other raster factors, the dataset was digitised, resampled, and standardised to match their spatial resolution and extent. The geological framework strongly controls groundwater distribution. Lithology, defined by the physical and chemical properties of rocks and sediments, influences key aquifer characteristics such as porosity, permeability, and storage capacity (Pandian & Kumanan, 2013). In this study, lithological data were converted from vector to raster format using GIS tools to enable spatial integration with other factors (Kumar et al., 2015). The dataset was reclassified into hydrogeologic response groups (e.g., permeable carbonates, fractured volcanics, low-permeability clays) according to groundwater relevance. The resulting lithological layer supports the identification of potential groundwater zones and clarifies geological controls on aquifer distribution (Fetter, 2018).

3.2.5. Precipitation

Monthly precipitation was obtained from NASA's POWER repository (products derived from CERES and MERRA-2). Data were downloaded as CSV, quality-checked (units, duplicates, outliers), projected to the study CRS, and imported to ArcGIS Pro.

A continuous precipitation surface was generated using IDW interpolation (power = 2; variable search radius, up to 12 neighbours), with cell size matched to the analysis grid and the output clipped to the study boundary. The resulting raster provides the spatial distribution of precipitation used as an input to the groundwater-recharge assessment.

3.2.6. Land use

Land use strongly influences hydrological processes by affecting infiltration, runoff, erosion, and evapotranspiration. Sentinel-2 MSI (Level-1C) imagery, processed on Google Earth Engine, was used to derive the land-use map. The dataset was reclassified in GIS into hydrologically relevant categories: bare soil, vegetation/agriculture, and built-up areas. This classification supports assessment of surface runoff and groundwater recharge dynamics.

3.2.7. Normalization (standardization) of factors

This linear normalization using to aggregate heterogeneous criteria. Each factor $x_{k(i)}$ was rescaled to a unitless suitability score $r_k(i) \in [0,1]$ on the common evaluation scale. Allowing comparison and integration of heterogeneous datasets (benefit-type criteria, where higher values are more favourable) Two monotonic transformations were used:

1. Benefit-type (larger is better; e.g., lineament density, precipitation):

$$r_k(i) = \frac{x_{k(i)} - min(x_k)}{max(x_k) - min(x_k)} \tag{4}$$

2. Cost-type (smaller is better; e.g., slope, drainage density when high values impede recharge):

$$r_k(i) = \frac{max(x_k) - x_{k(i)}}{max(x_k) - min(x_k)} \tag{5}$$

where:

- expert knowledge recommended non-linear responses, we used fuzzy membership $\mu k(x) \in [0,1]$,
- $r_k(i)$ – normalized (standardized) value of factor k at location i,
- $x_k(i)$ – original value of factor k at location i,
- $max(x_k)$, $min(x_k)$ – minimum and maximum values of factor k, respectively.

3. Piecewise linear (increasing benefit)

$$u_k(x) = \begin{cases} 0, x \le a \\ \frac{x-a}{b-a}, a < x < b \\ 1, x \ge b \end{cases} \tag{6}$$

4. Logistic (decreasing cost; e.g., slope)

$$u_k(x) = \frac{1}{1 + exp\langle -a(c-x)\rangle}, a > 0 \tag{7}$$

where:

- $u_k(x)$ – fuzzy membership value of factor k at value x, scaled to [0,1],
- a – slope (steepness) parameter controlling the curve shape,
- c – mid-point where $u_k(x) = 0.5$,
- x – raw value of the factor.

3.2.8. Weighting by AHP and pairwise-consistency checks

Relative factor importance was determined using the Analytic Hierarchy Process (AHP), a multi-criteria decision-making technique that quantifies expert judgments through pairwise comparisons (Table 1). In this approach, experts evaluated the relative influence of each conditioning factor on groundwater potential by comparing them two at a time based on their significance.

The comparisons were organized into a positive reciprocal matrix $A = (a_{ij})$, where each element a_{ij} represents the importance of factor i relative to factor j. Values were assigned using Saaty's 1–9 scale, in which 1 denotes equal importance, 3 moderate importance, 5 strong importance, 7 very strong importance, and 9 extreme importance; reciprocals (e.g., 1/3, 1/5) indicate lesser importance (Table 2) .

To better visualise these pairwise relationships, a heatmap (Fig. 5) was generated from the comparison matrix. This graphical representation highlights the relative intensity of influence between factors, with warmer colours indicating higher importance. The heatmap aids in quickly identifying dominant factors (such as precipitation and drainage density) and verifying the coherence of expert judgments across all criteria.

Once the matrix was constructed, weights (ω_k) representing the relative contribution of each factor were derived from the principal right eigenvector of matrix A, obtained by solving:

$$A_\omega = \lambda_{max}\omega, \sum_{k=1}^{m} \omega_k \tag{8}$$

where:

- λ_{max} – is the maximum eigenvalue of the matrix,
- $\sum_{k=1}^{m} \omega_k$ – (the resulting normalized weights) express the proportional influence of each factor in the groundwater potential assessment.

To verify the consistency of the expert judgments in the Analytic Hierarchy Process (AHP),

Table 1. The intensity of influence for each factor according to the method (AHP).

Factor A	Factor B	Preferred Factor	Intensity (1–9)
Precipitation	Drainage density	Precipitation	1
Precipitation	Lithology	Precipitation	1
Precipitation	Slope	Precipitation	2
Precipitation	Lineament density	Precipitation	3
Precipitation	Soil type	Precipitation	5
Precipitation	Land use	Precipitation	9
Drainage density	Lithology	Drainage density	2
Drainage density	Slope	Drainage density	3
Drainage density	Lineament density	Drainage density	3
Drainage density	Soil type	Drainage density	6
Drainage density	Land use	Drainage density	9
Lithology	Slope	Lithology	2
Lithology	Lineament density	Lithology	2
Lithology	Soil type	Lithology	3
Lithology	Land use	Lithology	8
Slope	Lineament density	Slope	1
Slope	Soil type	Slope	2
Slope	Land use	Slope	5
Lineament density	Soil type	Lineament density	2
Lineament density	Land use	Lineament density	5
Soil type	Land use	Soil type	2

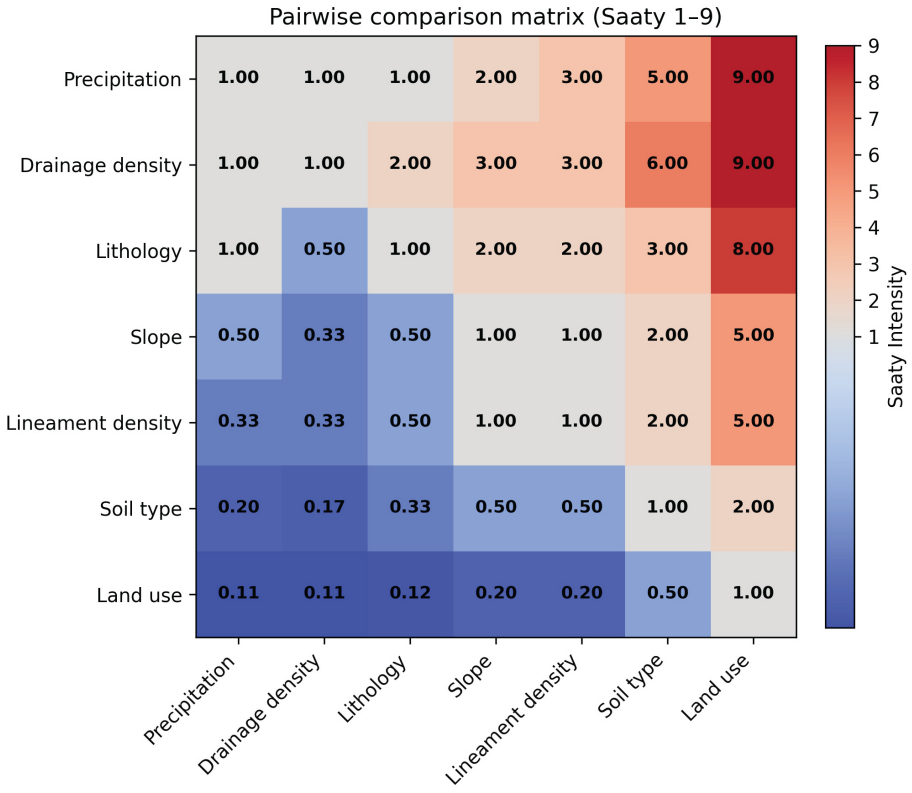

Fig. 5. Heatmap of pairwise comparison matrix showing intensity of factor importance.

Table 2. A scale for pairwise comparations and their definitions.

Name	Intensity	Explanation
Equal importance	1	The two elements contribute equally to the objective
Moderate importance	3	Experience and judgment slightly favor one element over the other
Strong importance	5	Experience and judgment clearly favor one element over the other
Very strong importance	7	One element is strongly favored; its dominance is demonstrated in practice
Extreme importance	9	Evidence favoring one element over the other is of the highest possible order

two key indicators were computed: the Consistency Index (CI) is defined as:

$$CI = \frac{\lambda_{max} - m}{m - 1} \qquad CR = \frac{CI}{RI},$$

- λ_{max} – maximum eigenvalue of the pairwise comparison matrix,
- m – number of factors (criteria) considered,
- RI – Random Consistency Index, whose value depends on mmm (e.g., RI = 1.49 for m = 10m).

Following refinement of a few pairwise judgments to improve coherence, the final matrix achieved a Consistency Ratio of CR = 0.008, indicating excellent consistency. After constructing the pairwise comparison matrix and verifying consistency (CR < 0.1), the normalized weights were derived from the principal eigenvector. The relative influence of each factor is presented in Table 3, while Figure 6 shows the contribution of each factor graphically.

Table 3. Effect of each influencing factor.

Factor	Influence (%)
Precipitation	24.13
Drainage density	29.01
Lithology	18.87
Slope	10.49
Lineament density	9.92
Soil type	5.12
Land use	2.46

3.2.9. Weighted factor classification

Each conditioning factor was reclassified into suitability classes based on its hydrological relevance and contribution to groundwater recharge. Classes were assigned verbal categories (excellent, very good, good, moderate, poor) and corresponding numeric scores (1–5), with higher scores indicating more favourable conditions for recharge (Table 4).

3.2.10. GIS-based weighted overlay (WLC)

The Groundwater Potential Zone (GPZ) was calculated using the Weighted Linear Combination (WLC) method applied to the normalized factor layers. Each factor's standardized value was multiplied by its respective weight, and the weighted values were summed across all factors:

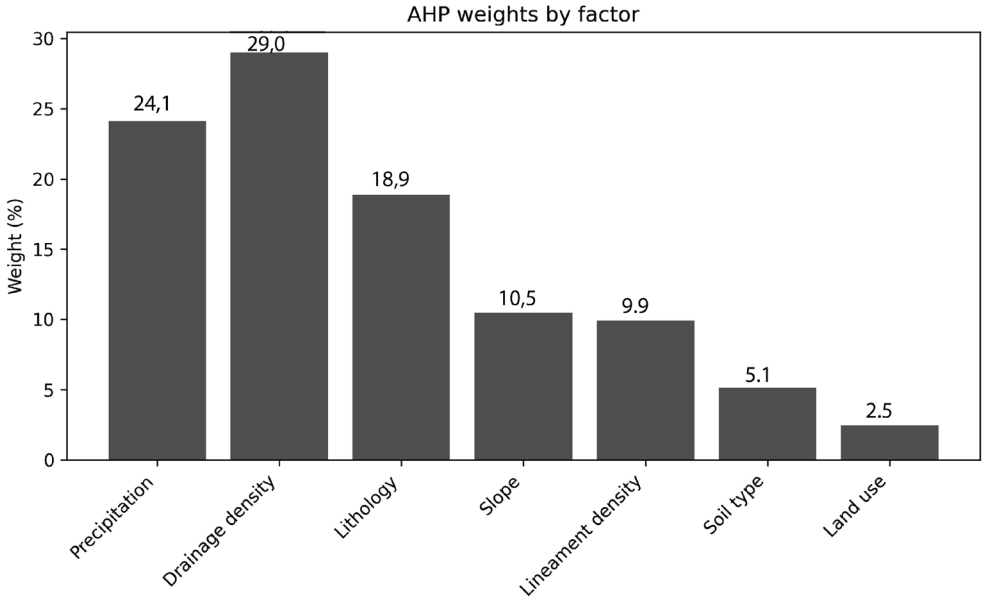

Fig. 6. The contribution of each factor.

Table 4. Weighted factors influencing groundwater recharge zones.

Factor	Class / Category	Verbal class	Numeric score	Weight (%)
Precipitation	1	Excellent	1	24.13
	2	Very good	2	
	3	Good	3	
	4	Moderate	4	
	5	Poor	5	
Lithology	Alluvium	Excellent	5	18.87
	Clay	Moderate	2	
	Conglomerate (regs, alluvial fans)	Excellent	5	
	Sandstone	Very good	4	
	Silt, conglomerate, alluvium	Excellent	5	
	Quartzite	Poor	1	
	Igneous rocks	Poor	1	
	Volcano-sedimentary rocks	Poor	1	
	Sand	Excellent	5	
	Schist	Moderate	2	
	Carbonate	Moderate	2	
Slope	1	Excellent	5	10.49
	2	Very good	4	
	3	Good	3	
	4	Moderate	2	
	5	Poor	1	
Drainage density	1	Excellent	5	29.01
	2	Very good	4	
	3	Good	3	
	4	Moderate	2	
	5	Poor	1	
Land use / land cover (LU/LC)	Built-up areas	Poor	1	2.46
	Water	Excellent	5	
	Vegetation	Excellent	5	
	Bare soil	Poor	1	
Lineament density	1	Poor	1	9.92
	2	Excellent	5	
Soil (WRB)	Acrisols	Moderate	2	5.12
	Calcisols	Good	3	
	Cambisols	Good	3	
	Fluvisols	Excellent	5	
	Gypsisols	Good	3	
	Leptosols	Good	3	
	Luvisols	Moderate	2	
	Regosols	Poor	1	

$$GPI(i) = \sum_{k=1}^{m} \omega_k r_k(i), \qquad \sum_{k=1}^{m} \omega_k = 1 \qquad (10)$$

where:
- $GPI(i)$ – groundwater potential score at location i,
- ω_k – relative weight of factor k,
- $r_k(i)$ – normalized (unitless) suitability value of factor k at location i,
- m – total number of conditioning factors.

This linear aggregation ensures that factors with higher influence (larger ωk) contribute more to the final index. The procedure was implemented in ArcGIS using the Weighted Overlay tool, which integrates the reclassified layers, assigned weights, and performs cell-wise aggregation on a common grid to produce the continuous GPZ map.

3.2.11. Demarcation of groundwater-potential zones

The continuous Groundwater Potential Zones (GPZ) raster was classified into five categories (very low, low, moderate, high, and very high) using the Jenks natural breaks method. This classifica-

tion approach optimizes groupings by maximizing variance between classes and minimizing variance within each class.

Let $t_0 < t_1 < \ldots < t_5$ denote the breakpoints determined by the Jenks algorithm. Each pixel was assigned to a class $C(i)$ according to:

$$C(i) = j \text{ if } t_{j-1} \leq GPI(i) < t_j,\ j = 1, \ldots, 5.$$

Breaks were reviewed against known hydrogeologic features; no manual edits were applied unless expert consensus indicated systematic bias.

4. Results

4.1. Overview of groundwater recharge potential

The integration of all thematic layers within the AHP-GIS framework generated the final groundwater recharge potential map (Fig. 8), which delineates four distinct classes: excellent, good, moderate, and poor. Areas of excellent and good potential are predominantly concentrated along the central axis of the basin, particularly following the course of the Drâa River, where gentle topography, permeable alluvial formations, and structural discontinuities enhance infiltration. Moderate-potential zones occupy the surrounding piedmonts, whereas poor-potential areas dominate the outer and southern margins of the basin, where arid conditions, steep slopes, and impermeable substrates restrict recharge. This spatial configuration reflects the combined influence of lithology, geomorphology, slope, and drainage characteristics. Validation data from ABHDON further support these patterns: wells situated within high-potential zones exhibit discharge rates exceeding 6 L/s, while those in moderate or poor sectors rarely surpass 1.5 L/s. The agreement between field observations and the modelled results attests to the reliability and consistency of the final recharge potential map.

4.2. Slope

Slope is one of the key factors controlling groundwater infiltration into the subsoil, making it an important indicator for assessing groundwater potential. In areas with gentle slopes, surface runoff is slow, allowing rainwater more time to infiltrate, whereas areas with steep slopes favour rapid runoff, reducing the residence time of rainwater and consequently decreasing infiltration. The slope map (Fig. 7A) shows that slope percentages in the region range from 0 to 52%. Areas with slopes between 0 and 2% are classified as excellent due to the flat terrain and relatively high infiltration rate. Areas with slopes between 2 and 5% are considered very good because of the nearly flat terrain and similarly high infiltration capacity. The majority of the study area (about 71%) falls within the 0–5% category. Areas with slopes between 5 and 8% are characterised by moderate runoff and good infiltration, and are therefore classified as good. Areas with slopes between 8 and 12% are considered moderate due to increased slope and higher runoff, while areas with slopes between 12 and 52% are considered poor because of the very steep terrain and rapid runoff. The distribution of slope classes in relation to recharge potential is shown in the figure below, and their areal distribution is illustrated in the pie chart.

4.3. Land use

The land-use map of the studied watershed (Fig. 7B) shows a heterogeneous distribution of land-cover types, reflecting both natural and anthropogenic influences. Bare lands account for the majority of the basin, covering over 90% of the area and being present throughout almost the entire territory. Built-up areas and urban expansion occupy approximately 5.67%, mainly represented by villages scattered along the valleys. Water bodies, including rivers and small reservoirs, cover the remaining 2.17%. Vegetation cover is very limited, representing only 1.3% of the basin, and is primarily concentrated in higher altitudes as well as along riverbanks forming oasis areas. The interaction between these three main classes and their spatial distribution collectively influences hydrological processes such as runoff, infiltration, and groundwater recharge.

4.4. Drainage density

The drainage-density map (Fig. 7C) reveals values ranging from 0 to 42.57 km/km^2, which have been reclassified into five classes: 0–3.5, 3.5–10, 10–16.7, 16.7–24, and 24–42.57 km/km^2. Spatial analysis shows that the first class (0–3.5 km/km^2), corresponding to areas with very low drainage density, covers about 30% of the total basin area. The second class (3.5–10 km/km^2) accounts for nearly 20%, indicating a low to moderate density. The third class (10–16.7 km/km^2) represents 24% of the area, while the fourth class (16.7–24 km/km^2) covers 17.17%.

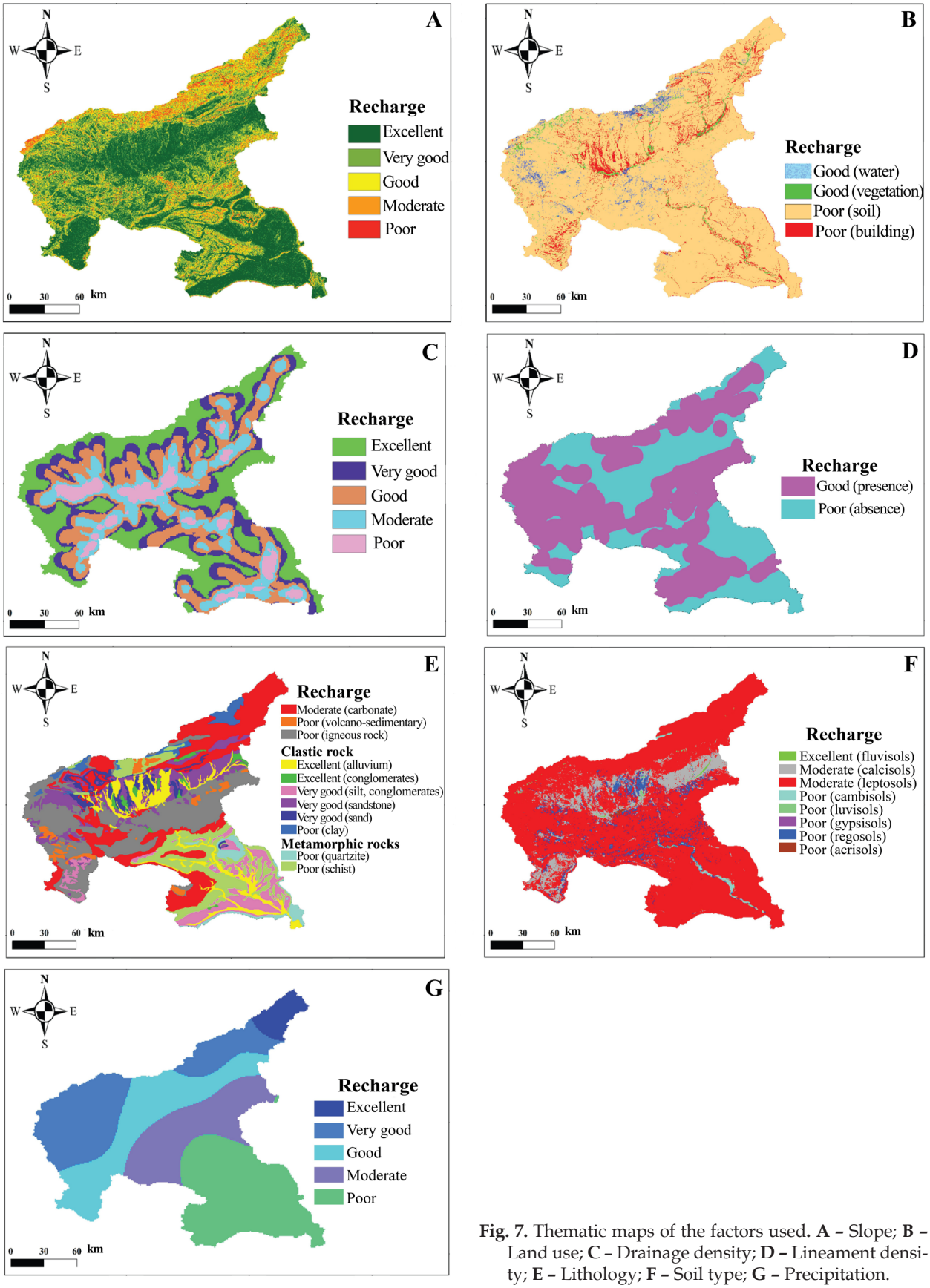

Fig. 7. Thematic maps of the factors used. **A –** Slope; **B –** Land use; **C –** Drainage density; **D –** Lineament density; **E –** Lithology; **F –** Soil type; **G –** Precipitation.

Finally, the last class (24–42.57 km/km^2), corresponding to areas with very high drainage density, occupies only 7.94% of the basin. From a recharge perspective, regions with very low drainage density are assigned a higher weight, whereas those with very high drainage density are assigned a lower weight. Based on the potential for groundwater recharge, drainage density is classified into five categories: excellent, very good, good, moderate and low.

4.5. Density of lineaments

The lineament-density map highlights a classification into two main classes (Fig. 7D). The first class corresponds to areas with a high presence of lineaments, covering 60.5 % of the total basin area. These lineaments are particularly concentrated in the northern part, within the High Atlas, and in the southern part, within the Anti-Atlas, areas characterised by high altitudes and structured relief. In contrast, the second class, exhibiting low lineament density, is mainly located in the central part of the basin and in a few scattered areas within the two mountain ranges, representing 39.51 % of the area. This spatial distribution suggests that geological structure and altitude play a major role in lineament distribution, potentially influencing groundwater recharge processes and the hydrogeological dynamics of the basin. The lineament density and its spatial distribution, considered major structural anomalies, influence flow dynamics and can affect groundwater recharge as well as the overall hydrogeological dynamics of the basin.

4.6. Lithology

Given that the basin covers a large area encompassing both the Atlassic and Anti-Atlasic domains, it exhibits a wide diversity of geological formations, expressed through the distinction of several lithological units with varying proportions (Fig. 7E). In the upstream part, corresponding to the Central High Atlas, the basin is mainly dominated by carbonate, marl, sandstone, and silt formations. Moving towards the middle zone, the lithology is characterised by the predominance of sandy and alluvial deposits infilling the topographic depression of the Ouarzazate Basin. Further south, the terrains are represented by igneous lithologies associated with the Anti-Atlas chain. Finally, in the downstream extremity, the outcrops consist of Palaeozoic quartzites and schists, along with recent alluvial deposits. This spatial distribution plays a key role in controlling surface runoff and groundwater recharge.

4.7. Soil

The soil type map shows that the watershed is composed of eight main classes, thereby reflecting a marked textural diversity (Fig. 7F). In terms of dominance, leptosols cover the largest portion of the basin, accounting for 82.95% of the total area, followed by calcisols with 11.54% and regosols with 4.5%. The other soil classes, namely acrisols, cambisols, fluvisols, gypsisols, and luvisols, occupy much smaller areas, each representing less than 1% of the basin. This distribution gives the watershed a particularly diverse pedological character.

4.8. Precipitation

In the study area, precipitation ranges from 70 to 339 mm per year (Fig. 7G), decreasing progressively from north to south as a result of latitude and basin topography. Areas receiving between 70 and 110 mm are classified as having 'low' recharge, since the limited rainfall reduces infiltration potential. Those with 110 to 156 mm are considered to have 'moderate' recharge, reflecting an average water supply. Zones receiving between 156 and 207 mm are classified as having 'good' recharge due to relatively high infiltration capacity, while those with 207 to 271 mm also show 'good' recharge but with an even stronger potential. Finally, areas with 271 to 339 mm of rainfall are classified as having 'excellent' recharge, owing to abundant precipitation that greatly enhances infiltration.

4.9. Potential groundwater recharge zones map

By integrating the previously described thematic maps, a final map of potential groundwater recharge zones was produced (Fig. 8), highlighting their spatial distribution within the basin. These zones were classified into four categories based on their recharge potential, namely excellent, good, moderate, and low. Zones with excellent and good potential are primarily concentrated in the central part of the basin, following the main watercourses that drain the study area. Moving away from this central zone, the recharge potential gradually decreases, falling into the moderate and low categories.

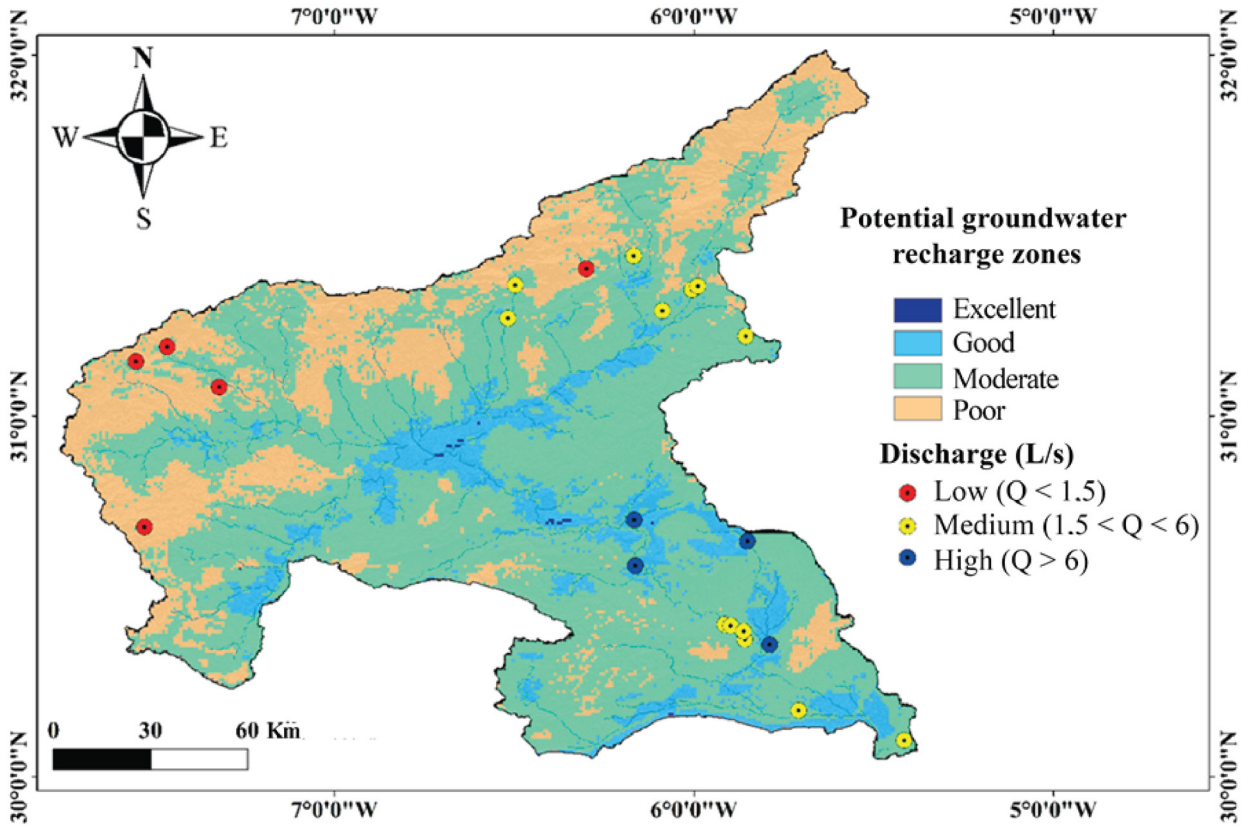

Fig. 8. Spatial distribution map of potential groundwater recharge zones.

These results were supported by field measurements of discharge taken at several representative points across the basin. The analysis indicates that the highest discharges, exceeding 6 L/s, occur in the central part of the basin. Conversely, as the distance from the centre increases, discharges gradually decrease, ranging from 1.5 L/s to 6 L/s, which corresponds to the spatial distribution of recharge potential. This consistency between the thematic maps and field measurements confirms the reliability of the recharge zone mapping.

5. Discussion

Groundwater recharge zones with high potential are mainly located in alluvial plains and fractured regions, corresponding to gentle slopes (0–5%). This distribution can be explained by the predominance of infiltration over surface runoff. Thus, areas with high potential are generally concentrated downstream from the Mansour Eddahbi Dam, forming a zonation along the Drâa Valley. This spatial pattern suggests that the origin of these waters is largely due to infiltration, particularly concentrated in topographic depressions. Certain parts of the Upper-Middle Drâa Basin, notably Agdz and Bouskour villages, have been identified as major recharge zones due to favourable geology and significant fracturing, which facilitate infiltration and efficient groundwater flow. In this context, the study by Boummane et al. (2009) on the Ouarzazate Basin demonstrated that the distribution and orientation of faults significantly influence groundwater movement. Similarly, areas with moderate potential located at the piedmont of the Atlasic chain, such as villages of Boumalne, Skoura, and Kelaat M'gouna, are supplied by faults and karstic flows characteristic of the limestones of the Central High Atlas. Moreover, Agoussine et al. (2004) emphasise that this recharge originates mainly from the Atlasic chain to the north, with a general flow direction toward the northeast. This explains the concentration of high-potential areas in low-altitude zones, as illustrated by the final map (Fig. 8).

The verification of these interpretations is essentially based on the analysis of borehole discharge data provided by the Hydraulic Agency of the Drâa-Oued Noun Basin (ABHDON). The spatial assessment of these data reveals a clear correlation between potential recharge zones and

high discharge values, indicating strong aquifer productivity in these areas. Conversely, a gradual decrease in discharge is observed toward the basin margins, reflecting a lower recharge potential and a less favourable hydrodynamic gradient. These findings are broadly consistent with results reported in similar hydrogeological contexts in Morocco and neighbouring regions. For example, Ikirri et al. (2023) identified the most favourable recharge zones in the Ifni Basin (Western Anti-Atlas) within alluvial and fractured terrains, where infiltration dominates over runoff, which is a pattern closely resembling that of the Drâa Basin. Likewise, Seqqam et al. (2025) in the Khouribga area and Hairchi et al. (2025) in the Guigou Basin (Middle Atlas) emphasised the combined control of lithology, slope, and drainage density on recharge, confirming the influence of structural and geomorphological factors observed in this study. Beyond Morocco, studies such as Melese & Belay (2022) (Ethiopia), and Pirasteh et al. (2025) (India) also reported similar correlations between gentle slopes, fractured rocks, and high recharge potential, validating the robustness of the AHP approach across different hydroclimatic settings. In arid Morocco, Elmotawakkil et al. (2025) applied a deep learning framework in the Feija Basin and likewise found that recharge potential concentrates in low-lying and vegetated areas with permeable formations, which is a trend that reinforces the spatial coherence of our own results across the southern basins. However, the present study distinguishes itself by the large spatial extent of the investigated area (Upper-Middle Drâa Basin), covering diverse geomorphological and climatic zones from the High Atlas piedmont to the pre-Saharan plains. This broad coverage adds complexity but also ensures a comprehensive understanding of recharge dynamics across contrasting environments.

The application of the AHP method at this scale demonstrates its reliability and adaptability to heterogeneous arid terrains, where data availability often remains limited. Overall, the coherence between our results and previous studies underlines the validity of the adopted approach and the regional consistency of recharge mechanisms in arid and semi-arid Moroccan basins. The integration of remote sensing and GIS with the AHP model has proven efficient for identifying recharge-prone areas, even in data-scarce regions. Nonetheless, some limitations persist, particularly regarding the temporal updating of field data and the lack of continuous monitoring of piezometric levels and discharges. Future work should incorporate higher-resolution hydrogeological and climatic datasets, extended time-series analyses, and complementary machine learning approaches to refine recharge zone delineation and improve the predictive capacity of spatial models in complex arid systems.

6. Conclusions

In conclusion, the present study enabled the mapping of high groundwater recharge potential zones in the Upper-Middle Drâa Basin using the Analytic Hierarchy Process (AHP) combined with GIS and Sentinel-2 satellite imagery. The integration and overlay of thematic maps, including lineament density, drainage density, slope gradient, land use, soil type, lithology, and precipitation, allowed the production of a final map reflecting the recharge potential of different areas. The results indicate that high-potential zones are mainly located in low-altitude areas at the centre of the basin, highlighting the significant influence of topography, precipitation, and drainage density on the spatial distribution of recharge zones. The correlation of these results with field data shows a satisfactory agreement, confirming the reliability of the adopted method. However, certain limitations remain, notably the resolution of satellite data, the lack of piezometric measurements, and the need to account for seasonal variations in precipitation, which could affect the distribution of zones with high groundwater recharge potential.

Acknowledgements

We express our deep gratitude to the anonymous reviewers for their constructive comments and suggestions, as well as to the journal editor for the thorough screening, which greatly contributed to improving the clarity and quality of the manuscript.

Author's contributions:

HG: Conceptualization, methodology, software, resources, investigation, validation, writing – original draft. AT, AA and SM: Investigation, validation, and visualisation. ME: Methodology, investigation.

Conflict of interest

On behalf of all authors, the corresponding author states that there is no conflict of interest.

References

Agoussine M., El M., Saidi M. & Igmoullan B., 2004. *Reconnaissance des ressources en eau du bassin d ' Ouarzaz-*

ate [*Recognition of water resources in the Ouarzazate basin*]. [In:] Lias sources and documents relating to the early modern history of ideas. 81–92 pp.

Arulbalaji P., Padmalal D. & Sreelash K., 2019. GIS and AHP techniques based delineation of groundwater potential zones: a case study from southern Western Ghats, India. *Scientific Reports* 9, 2082.

Benchattou A. & El Ghachi M., 2024. *Climate change projection and numerical climate modeling in the Rheris Watershed* (*Region Drâa Tafilalet – Morocco*). [In:] Climate change effects and sustainability needs: The case of Morocco. Springer. 35–44 pp.

Benvenuti M., Moratti G. & Algouti A., 2017. Stratigraphic and structural revision of the Upper Mesozoic succession of the Dadès valley, eastern Ouarzazate Basin (Morocco). *Journal of African Earth Sciences* 135, 54–71. https://doi.org/10.1016/j.jafrearsci.2017.01.018

Bouchaou L., Michelot J.L., Qurtobi M., Zine N., Gaye C.B., Aggarwal P.K., Marah H., Zerouali A., Taleb H. & Vengosh A., 2009. Origin and residence time of groundwater in the Tadla basin (Morocco) using multiple isotopic and geochemical tools. *Journal of Hydrology* 379, 323–338.

Boummane K., Jaffal M. & Kchikach A., 2009. Study of the Ouarzazate Basin structure by seismic reflection: Hydrogeological implications. *Estudios Geologicos* 65, 157–165. https://doi.org/10.3989/egeol.39864.065

Cappy S., 2006. *Hydrogeological characterization of the Upper Drâa catchment: Morocco*. 41–68 pp.

Diriba D., Karuppannan S., Takele T. & Husein M., 2024. Delineation of groundwater potential zonation using geoinformatics and AHP techniques with remote sensing data. *Heliyon* 10 (3).

DRPE, 1994. *Master plan study for the development of the Guir, Ziz, Rhéris and Drâa basins: development scheme study*. *Vol. II.* Direction of Water Research and Planning. Rabat, Morocco.

DRPE, 2010. *Master plan study for the development: the Guelmim Hydraulic Basin*. *Vol. II.* Direction of Water Research and Planning. Rabat, Morocco.

Duguma T.A. & Duguma G.A., 2022. Assessment of groundwater potential zones of upper blue nile river basin using multi□influencing factors under GIS and rs environment: a case study on guder watersheds, abay basin, Oromia region, Ethiopia. *Geofluids* 1172039.

Elmotawakkil A., Moumaneb A., Zahi A., Sadiki A., Karkouri J., Batchi M., Bhagat S.K., Tiyasha T. & Enneya N., 2025. Artificial intelligence for groundwater recharge prediction in an arid region: application of tabular deep learning models in the Feija Basin, Morocco. *Frontiers in Remote Sensing* 6, 1622360.

Ervin M.C. & Morgan J.R., 2001. Groundwater control around a large basement. *Canadian Geotechnical Journal* 38, 732–740.

Fekkak A., 1992. *Le PII. Inférieur de la boutonniere de sidi flah* (*Saghro Occidental, Anti-Atlas, Maroc*)*: Relique d'un substratum océanique de l'arc du Saghro* [Lower part of the Sidi Flah (Western Saghro, Anti-Atlas, Morocco): Relic of an oceanic bedrock of the Saghro arc]. University Cadi Ayyad, Marrakech. 83–92 pp.

Fetter C.W., 2018. *Applied Hydrogeology*. 4th ed. Waveland Press, 284 pp.

Gebru H., Gebreyohannes T. & Hagos E., 2020. Identification of groundwater potential zones using analytical hierarchy process (AHP) and GIS-remote sensing integration, the case of Golina River Basin, Northern Ethiopia. *International Journal of Advanced Remote Sensing and GIS* 9, 3289–3311.

Gintamo B., Khan M.A., Gulilat H., Shukla R.K. & Mekonnen Z., 2022. Determination of the physicochemical quality of groundwater and its potential health risk for drinking in Oromia, Ethiopia. *Environmental Health Insights* 16, 11786302221096052.

Hairchi K. El, Limame A., Benbrahim Y., Saadi O., Ouiaboub L., Nouayti A. & Nouayti N., 2025. Groundwater potential zones mapping using GIS, RS, and AHP method in the Guigou basin, Middle Atlas, Morocco. *Euro-Mediterranean Journal for Environmental Integration* 10, 703–719.

Ikirri M., Boutaleb S., Ibraheem I.M., Abioui M., Echogdali F.Z., Abdelrahman K., Id-Belqas M., Abu-Alam T., El Ayady H. & Essoussi S., 2023. Delineation of groundwater potential area using an AHP, remote sensing, and GIS techniques in the Ifni Basin, Western Anti-Atlas, Morocco. *Water* 15, 1436.

Jossen J.A. & Filali Moutei J., 1988. Ouarzazate Basin, stratigraphic and structural synthesis. *Contribution à l'étude Des Aquifères Profonds–Projet PNUD–DRPE* (*Direction de La Recherche et de La Planification de l'Eau*) *MOR/86/004-Exploration Des Eaux Profondes. Rapport Inédit, Rabat*.

Kumar D. & Ahmed S., 2003. Seasonal behaviour of spatial variability of groundwater level in a granitic aquifer in monsoon climate. *Current Science*, 188–196.

Kumar N., Yamaç S.S. & Velmurugan A., 2015. Applications of remote sensing and GIS in natural resource management. *Journal of the Andaman Science Association* 20, 1–6.

Lee S. & Pradhan B., 2007. Landslide hazard mapping at Selangor, Malaysia using frequency ratio and logistic regression models. *Landslides* 4, 33–41.

Machiwal D., Jha M.K. & Mal B.C., 2011. Assessment of groundwater potential in a semi-arid region of India using remote sensing, GIS and MCDM techniques. *Water Resources Management* 25, 1359–1386.

Melese T. & Belay T., 2022. Groundwater potential zone mapping using analytical hierarchy process and GIS in Muga Watershed, Abay Basin, Ethiopia. *Global Challenges* 6, 2100068.

Moges D.M. & Bhat H.G., 2017. Integration of geospatial technologies with RUSLE for analysis of land use/cover change impact on soil erosion: case study in Rib watershed, north-western highland Ethiopia. *Environmental Earth Sciences* 76, 765.

Murmu P., Kumar M., Lal D., Sonker I. & Singh S.K., 2019. Delineation of groundwater potential zones using geospatial techniques and analytical hierarchy process in Dumka district, Jharkhand, India. *Groundwater for Sustainable Development* 9, 100239.

Oikonomidis D., Dimogianni S., Kazakis N. & Voudouris K., 2015. A GIS/remote sensing-based methodology

for groundwater potentiality assessment in Tirnavos area, Greece. *Journal of Hydrology* 525, 197–208.

Olubusola I.S., Isaac A., Oyamenda O.K. & Adesola B.M., 2023. Assessment of groundwater occurrence in a typical schist belt region in Osun State, Southwestern Nigeria using VES, aeromagnetic dataset, remotely sensed data, and MCDA approaches. *Sustainable Water Resources Management* 9, 29.

Oukhro R., Youbi N., Kalderon-Asael B., Evans D.A.D., Pierce J., Wotzlaw J.-F., Ovtcharova M., Mata J., Mediany M.A. & Ounar J., 2025. Volcanic stratigraphy, petrology, geochemistry and precise U-Pb zircon geochronology of the Late Ediacaran Ouarzazate Group at the Oued Dar'a Caldera: Intracontinental felsic super-eruptions in association with continental flood basalt magmatism on the We. *Minerals* 15, 776.

Pandian M. & Kumanan C.J., 2013. Geomatics approach to demarcate groundwater potential zones using remote sensing and GIS techniques in part of Trichy and Karur district, Tamilnadu, India. *Archives of Applied Science Research* 5, 234–240.

Pirasteh S., Samad A., Ahmad R., Thakural L.N., Khan H.H., Chauhan P., Khan A. & Qamar M.Z., 2025. Geospatial and AHP based identification of potential zones for groundwater recharge in Haridwar District of India. *Frontiers in Environmental Science* 13, 1421918.

Priyan K., 2021. Issues and challenges of groundwater and surface water management in semi-arid regions. *Groundwater Resources Development and Planning in the Semi-Arid Region*, 1–17. https://doi.org/10.1007/978-3-030-68124-1_1

Saaty T.L. & Wind Y., 1980. Marketing applications of the analytic hierarchy process. *Management Science* 26, 641–658.

Schiavo A., Taj Eddine K., Algouti A., Benvenuti M., Vittorio G., Piaz D., Eddabbi A. & El Boukhari A., 2007. *Explanatory note. Geological map of Morocco 1:50,000, sheet Imtir*.

Sener E. & Davraz A., 2013. Assessment of groundwater vulnerability based on a modified DRASTIC model, GIS and an analytic hierarchy process (AHP) method: the case of Egirdir Lake basin (Isparta, Turkey). *Hydrogeology Journal* 21, 701–714.

Seqqam A., Touirsi M., Najib S., Fadili A. & Mehdi K., 2025. Integrated approaches to map groundwater potential zones using AHP, GIS, and remote sensing in semi-arid region of Morocco : Case study from Khouribga area. *Solid Earth Sciences* 10, 100272. https://doi.org/10.1016/j.sesci.2025.100272

Tolche A.D., 2021. Groundwater potential mapping using geospatial techniques: a case study of Dhungeta-Ramis sub-basin, Ethiopia. *Geology, Ecology, and Landscapes* 5, 65–80.

Tuduri J., Chauvet A., Barbanson L., Bourdier J.-L., Labriki M., Ennaciri A., Badra L., Dubois M., Ennaciri-Leloix C. & Sizaret S., 2018. The Jbel Saghro Au (Ag, Cu) and Ag–Hg metallogenetic province: product of a long-lived Ediacaran tectono-magmatic evolution in the Moroccan Anti-Atlas. *Minerals* 8, 592.

Uc Castillo J.L., Martínez Cruz D.A., Ramos Leal J.A., Tuxpan Vargas J., Rodríguez Tapia S.A. & Marín Celestino A.E., 2022. Delineation of groundwater potential zones (GWPZs) in a semi-arid basin through remote sensing, GIS, and AHP approaches. *Water* 14, 2138.

Manuscript submitted: 1 October 2025
Revision accepted: 5 November 2025